PERGAMON

International Journal of Heat and Mass Transfer 44 (2001) 2357–2373

International Journal of HEAT and MASS TRANSFER

www.elsevier.com/locate/ijhmt

Numerical study of high heat flux pool boiling heat transfer

Ying He [a,*], Masahiro Shoji [b], Shigeo Maruyama [c]

[a] *Department of Social Information Science, School of Integrated Sciences, Ochanomizu University, Room 409, Building No. 3, 2-1-1 Otsuka, Bunkyo-ku, Tokyo 112-8610, Japan*

[b] *Department of Mechanical Engineering, The University of Tokyo, 7-3-1 Hongo, Bunkyo-ku, Tokyo 113-8656, Japan*

[c] *Engineering Research Institute, The University of Tokyo, 2-11-16 Yayoi, Bunkyo-ku, Tokyo 113-8656, Japan*

Abstract

A new numerical simulation model of boiling heat transfer is proposed based on a numerical macrolayer model [S. Maruyama, M. Shoji, S. Shimizu, A numerical simulation of transition boiling heat transfer, in: Proceedings of the Second JSME–KSME Thermal Engineering Conference, pp. 3-345-3-348, 1992]. In this model, the boiling curve is reproduced numerically by determining the macrolayer thickness. It is found that the evaporation due to the growth of vapor stem is the main contribution to the total heat flux. In addition, the formation of nucleation site density is considered and the effect of surface roughness is investigated. Furthermore, the model is applied in the transient boiling process. The transient boiling curves are predicted through increasing power linearly and exponentially. The saturated liquid fluorinert FC-72 and water are used in the numerical calculation. Finally, this model is combined with three-dimensional transient heat conduction to investigate the spatial variations of wall temperature.

1. Introduction

Boiling is a complex and elusive process. For the past several decades, numerous investigations of modeling efforts on nucleate boiling have been carried out. According to the hypothesis on the heat transfer, these models may be divided into three major categories: bubble agitation models, vapor–liquid exchange models and latent heat and macro/microlayer evaporation models.

The bubble agitation models are based on the assumption that processes of bubble growth and release induce the surrounding liquid to the heat transfer process. The main role of the bubble is to agitate the liquid, but to carry away little heat. These kinds of models consider the heat transfer as the turbulent forced convection. The pool boiling heat transfer is correlated as the relationship between Nusselt number and Reynolds number [2,3]. The representative models are Rohsenow's model [4] and Zuber's microconvection model [5].

In the vapor–liquid exchange models, the movement of the vapor is postulated as microscopic pumps. When a bubble releases from the heated surface, it pushes the superheated liquid from the near-wall region into the cooler ambient and draws the cold fluid to the surface. At this time strong convective heat transfer is carried out between cold and superheated liquid. However, the temperature boundary layer is usually much less than the diameter of bubble, so the heat carried through the boundary layer will be limited. This kind of model may be far from the reality [2,3].

Recently, many researchers have shown that the evaporation of the liquid macro/microlayer plays an important role, especially at high heat flux regime. The liquid layer includes the microlayer underneath the bubble and the macrolayer at the base of coalescence bubble.

On the other hand, the representative mechanisms responsible for the critical heat flux (CHF) are Helmholtz-instability mechanism and the liquid macro/microlayer evaporation mechanism.

Zuber [6,7] originally put forward a CHF theoretical model based on Taylor instability and Helmholtz

* Corresponding author. Tel.: +81 48 476 6899; fax: +81 48 476 6899.

E-mail address: sjh_he@hotmail.com (Y. He).

0017-9310/01/$ - see front matter
PII: S0017-9310(00)00269-6

Nomenclature

A	area
A_v	area covered by vapor stems
A_w	total area of heater
D_c^*	diameter of cavity
g	gravitational acceleration
H	heater thickness
H_{fg}	latent heat of evaporation
i, j, k	coordinate indices in x, y, z directions
L	heater length
N	number of molecules per volume
N_s	number of surface cavity
q	instantaneous heat flux
q_{av}	time averaged heat flux
q_{CHF}	critical heat flux
q_{in}	input heat flux
$q_\alpha, \bar{q}_\alpha$	instantaneous and averaged heat flux component due to the increase of void fraction, respectively
$q_\delta, \bar{q}_\delta$	instantaneous and average heat flux component due to the decay of the macrolayer thickness, respectively
q_m	Gambill–Lienhard upper limit heat flux
Q	heat transfer rate
r_s	radius of a vapor stem
R	ideal gas constant
R_{ca}	cavity mouth radius
t	time
t_0	exponential period in Fig. 11
T_0	initial averaged surface temperature
T_b	temperature boundary condition at the bottom of the heater
T_{rate}	wall temperature heating rate in transient boiling
T_s	surface temperature
v_l	volumetric growth rate of bubble
w	equivalent macrolayer thickness
x, y, z	rectangular coordinates

Greek symbols

α	void fraction
α_l	thermal diffusivity
δ_0	initial macrolayer thickness
δ	instantaneous macrolayer thickness
δ_m	macrolayer thickness corresponding to q_m
ε	convergence coefficient
Δm	mass velocity of evaporated molecules
Δt	time step
ΔT_{act}	active wall superheat corresponding to a cavity
ΔT	wall superheat
λ	thermal conductivity of water
λ_H	thermal conductivity of heater
θ	contact angle
ρ_l	density of liquid
ρ_v	density of vapor
σ	surface tension
τ	bubble departure period
ξ	volumetric ratio of the accompanying liquid to the moving bubble

Subscripts

0	initial
av	average
b	bottom boundary
cal	calculated value
h	heater
l	liquid
m	maximum limit of evaporation
s	boiling surface
v	vapor
w	heated surface
P	present

Superscripts

$m, m+1$	computational times
$n, n+1$	time indices

instability. The fundamental idea is that the vapor generated at the flat plate accumulates to form the large continuous columns. CHF takes place when the vapor–liquid interface of the escaped passage becomes unstable due to Helmholtz instability. The equation is

$$q_{CHF} = \frac{\pi}{24}\rho_v H_{fg}\left[\frac{\sigma_g(\rho_l - \rho_v)}{\rho_v^2}\right]^{1/4}. \quad (1)$$

Bubble agitation mechanism and Helmholtz-instability mechanism can either explain most of heat transfer at the low heat flux regime or CHF, however, they cannot account for the continuity of the pool boiling curve. At this point, macro/microlayer evaporation mechanism is reasonable because it can reproduce the pool boiling curve from the nucleate boiling to transition boiling. Therefore, in the recent decades, numerous experimental and modeling efforts on liquid layer evaporation mechanism were carried out . Two main different postulates on the evaporation of liquid layer can be divided: the macrolayer model and the liquid–solid contact model.

Haramura and Katto [8] and Pan et al. [9] suggested an alternate CHF theory based on the role of the macrolayer. These models retained the basic element of Zuber's model [6,7] that hydrodynamic instabilities dictate the occurrence of CHF. However, they proposed

that the controlling instabilities occur not at the walls of large vapor columns but rather at the walls of tiny vapor stems around active nucleate cavities that intersperse the liquid macrolayer on the heater surface itself [10].

Bhat et al. [11] put forward a theoretical model of macrolayer formation. They suggested that active site density might play a role in high-heat flux nucleate boiling and CHF.

In the above models, the periodic supply of macrolayer liquid layer is considered to be the main mechanism of nucleate boiling and CHF.

On the other hand, in some models, the evaporation of micro liquid layer and the increasing of dry area of individual bubbles are considered to be important in nucleate boiling heat transfer. Dhir and Liaw [12] showed this idea in their time-averaged model. In their model, the heat from the wall is conducted into liquid macro/micro layer surrounding the stems and is utilized in evaporation at the stationary liquid–vapor interface. Later, Nagai and Nishio [13] pointed out that the growth of the primary isolated dry area was the mechanism of CHF according to their observations through a single crystal sapphire boiling surface. Zhao et al. [14] suggested the same viewpoint in their microlayer model.

Although these models can explain CHF and transition boiling fairly well, there appears to be some discrepancies among these models.

Maruyama et al. [1] presented a numerical model based on the macrolayer theory. The model retains the basic idea of Haramura and Katto's model [8] that the macrolayer forms underneath the coalesced bubble and dries out periodically. The difference is about the assumption of vapor stems. The model postulates that vapor stems are formed on the active cavity sites with a certain contact angle and the evaporation also occurs at the liquid–vapor interface. However, Haramura and Katto [8] assumed that the liquid–vapor interface was stationary and the entire surface heat flux contributed to macrolayer evaporation. In the study of Maruyama et al. [1], they firstly assumed an initial spatial pattern of vapor stems and employed the experimental macrolayer thickness with wall superheat. Subsequently, they calculated the heat flux according to their model and obtained the simulated boiling curve of water. In addition, they compared Haramura and Katto's model [8] and Dhir and Liaw's model [12]. The results show the compatibility with the two models. In fact, this model can be considered to be the combination of the spatial-averaged and time-averaged model.

Although the model by Maruyama et al. [1] combined the two kinds of viewpoints, there remain some problems that can be classified as:

1. The initial macrolayer thickness is determined by empirical wall superheat, which could not be easily generated.
2. It is obscure in dealing with the delay time for the vapor bubble formation which may have an effect on steady-state and transient boiling.
3. The wall temperature is assumed to be uniform.
4. The effect of surface roughness is not considered.

Recently, many researchers are trying to look for a valid numerical method to simulate boiling heat transfer. Pasamehmetoglu [15,16] developed a computer program to analyze low heat flux nucleate boiling. They simulated the bubble dynamics on the boiling surface by solving 3D transient heat conduction equation. The cylindrical control volumes with octagonal and square cross-sections in lateral and vertical directions, respectively were used in the simulation. Each octagonal cell was assumed to contain a nucleation cavity and representing the footprint of a departing bubble.

Bai and Fujita [17] performed a numerical simulation of a single bubble by combining hydrodynamics and heat transfer behavior. It was assumed that the evaporation heat was supplied from the superheated layer around the bubble by convection and from the meniscus part of the microlayer. Two-dimensional transient equations of mass, momentum and energy were solved by arbitrary Lagrangian–Eulerian finite element method (ALE-FEM). The growth process of an isolated bubble was simulated continuously. Son and Dhir [18] carried out similar work associated with a single bubble.

Lately, coupled mapping lattice (CML) [19,20] and lattice gas automata (LGA) [21] method were also applied in boiling simulation. Although CML and LGA reproduced different boiling modes and full boiling curve, at present the methods can only simulate boiling phenomena qualitatively.

In summary, more researchers came to pay attention to the numerical simulation of boiling and tried to find more information, which may be difficult to be found by experiments.

As there are still many arguments on macro/microlayer evaporation mechanism, we tried to use the numerical methods to develop a macrolayer model and investigate the unity between the macrolayer and liquid–solid contact model.

In this paper, we developed the model of Maruyama et al. [1] in order to reproduce the boiling curve numerically. Based on their physical model, we used a simple numerical method and fewer empirical relations to determine the wall superheat from the heat flux. In addition, the formation of nucleation site density is included to investigate the effect of surface cavities. Furthermore, the model is applied in the transient boiling process. The transient boiling curves are predicted through increasing power linearly and exponentially. Finally, the partial numerical method is used to investigate the spatial variations of wall temperature.

2. The developed numerical model

2.1. Governing equations

In this model, the basic physical model and equations of Maruyama et al. [1] are used. Fig. 1 shows the schematic of the top and side views of a vapor bubble on a heated surface. In this model, the macrolayer containing vapor stems occupies the region immediately next to the wall. The vapor stems are formed on the active cavity sites. The most important feature of this model is the introduction of a liquid–vapor stem interface evaporation phenomenon, which means that the evaporation occurs not only at the vapor bubble–macrolayer interface, but also at the stem interface.

In the first part of the study, as done in the model of Maruyama et al., we assumed the wall temperature was uniform and constant. The influence of temperature variation in the heater was not considered. From the heater surface heat is conducted into the macrolayer and is utilized in evaporation at the macrolayer–bubble interface. Therefore, the heat balance is written as

$$-\rho_l H_{fg}\frac{d\delta}{dt}=\frac{\lambda\Delta T}{\delta}. \tag{2}$$

By the integration of Eq. (2), the thickness of macrolayer can be obtained as

$$\delta(t)=\sqrt{\delta_0^2-2\frac{\lambda\Delta T}{\rho_l H_{fg}}t}. \tag{3}$$

The rate of heat transfer from the liquid–vapor stem interface can be written as

$$Q=\int q\,dA=\int_{r_0}^{r_1} q2\pi r\,dr$$
$$=2\pi r_0\lambda\Delta T\frac{1}{\tan\theta}\left[1+\left(\frac{\delta}{r_0\tan\theta}\right)+\log\left(\frac{\delta}{\delta_m}\right)\right], \tag{4}$$

where A is the liquid–vapor stem interface area. Suppose that heat from the heated surface is conducted into the interface area and is applied in the evaporation at the stem-liquid interface, the evaporated heat just contributes to the increase of radius of the vapor stem. Therefore, the heat balance equation can be expressed as

$$\int q\,dA=\rho_l H_{fg}A\frac{dr_s}{dt}\sin\theta, \tag{5}$$

where θ is defined as the contact angle in the model. The growth rate of vapor stems dr_s/dt is then obtained from

$$\frac{dr_s}{dt}=\frac{1}{\rho_l H_{fg}}\frac{\lambda\Delta T}{\delta}\left[1+\log\left(\frac{\delta}{\delta_m}\right)\right], \tag{6}$$

where δ_m is the thickness corresponding to the maximum evaporation heat flux for saturated pool boiling. The introduction of δ_m is to avoid the infinite heat flux at the

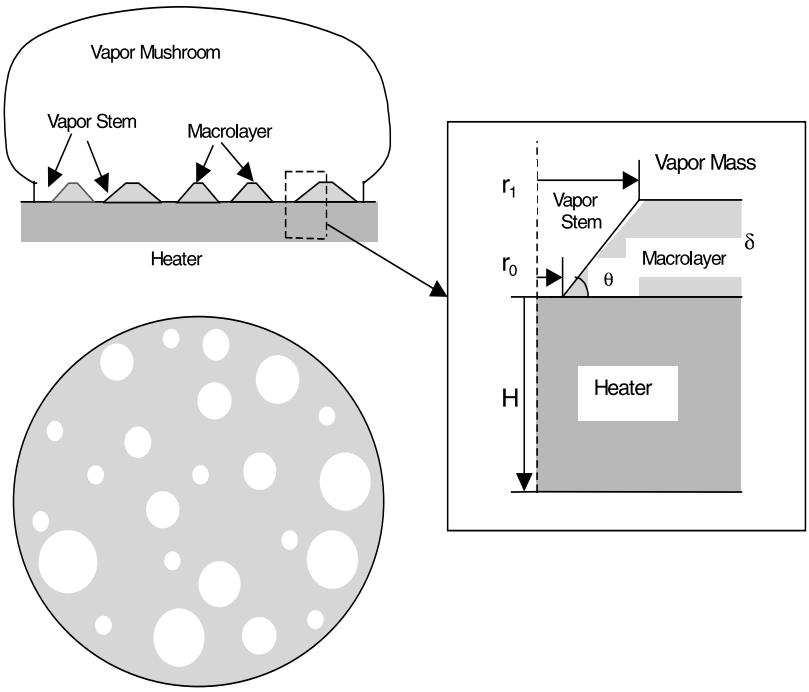

Fig. 1. Schematic of macrolayer model.

liquid–vapor interface. The maximum evaporation heat flux can be obtained by considering the evaporation and condensation of molecules. The upper limit heat flux thus is written as

$$q_{\mathrm{m}} = \Delta m H_{\mathrm{fg}} = \frac{\rho_{\mathrm{l}}}{\rho_{\mathrm{l}} - \rho_{\mathrm{v}}} \frac{\rho_{\mathrm{v}} H_{\mathrm{fg}}}{T_{\mathrm{sat}}} \frac{H_{\mathrm{fg}}}{\sqrt{2\pi R T_{\mathrm{sat}}}} \Delta T. \tag{7}$$

For saturated pool boiling of water at atmospheric pressure, the upper limit heat flux is

$$q_{\mathrm{m}} = 7.86 \Delta T \ (\mathrm{MW/m^2}). \tag{8}$$

Therefore, δ_{m} can be written as

$$\delta_{\mathrm{m}} = \frac{\lambda \Delta T}{q_{\mathrm{m}}}. \tag{9}$$

The instantaneous heat flux can be obtained as

$$\begin{aligned} q &= \rho_{\mathrm{l}} H_{\mathrm{fg}} \left(-\frac{\mathrm{d}w}{\mathrm{d}t} \right) \\ &= \rho_{\mathrm{l}} H_{\mathrm{fg}} (1-\alpha) \left(-\frac{\mathrm{d}\delta}{\mathrm{d}t} \right) + \rho_{\mathrm{l}} H_{\mathrm{fg}} \delta \frac{\mathrm{d}\alpha}{\mathrm{d}t} = q_{\delta} + q_{\alpha}, \end{aligned} \tag{10}$$

where the parameter w is defined as the equivalent thickness. It means the amount of liquid left on the surface. It is expressed as

$$w = \delta(1-\alpha), \tag{11}$$

q_{δ} and q_{α} are the heat fluxes related to the decay of macrolayer thickness and the growth of vapor stems, respectively.The macrolayer theory considers that the liquid supply occurs periodically and the departure period exactly corresponds to the sustained period of vapor bubble. Therefore, the averaged heat flux is expressed as

$$q_{\mathrm{av}} = \frac{1}{\tau} \int_0^{\tau} q \, \mathrm{d}t. \tag{12}$$

2.2. Closure relationships

With respect to the initial void fraction, Gaertner [22] showed that the diameter of the vapor stems had the relationship with the active site population for water as

$$D^2 \frac{N}{A} = \frac{1}{9}, \tag{13}$$

where D is the diameter of the vapor stem, N/A is the active site population. When vapor stems are formed directly, the diameters of the vapor stems are controlled within 0.4 mm according to the experiment [23].

Rajavanshi et al. [24] put forward an equation about initial macrolayer thickness according to Haramura and Katto's hypothesis [8], it is written as

$$\delta_0 = 0.0107 \sigma \rho_{\mathrm{v}} \left(1 + \frac{\rho_{\mathrm{v}}}{\rho_{\mathrm{l}}} \right) \left(\frac{\rho_{\mathrm{v}}}{\rho_{\mathrm{l}}} \right)^{0.4} \left(\frac{H_{\mathrm{fg}}}{q_{\mathrm{av}}} \right)^2. \tag{14}$$

In this simulation, for a given heat flux, the initial macrolayer thickness is obtained by Eq. (14). In the transition boiling regime, the extrapolated values of the equation are employed as the initial macrolayer thickness. The bubble departure period is according to the equation of Katto and Yokoya [25], i.e.,

$$\tau = \left(\frac{3}{4\pi} \right)^{1/5} \left[\frac{4(\xi \rho_{\mathrm{l}} + \rho_{\mathrm{v}})}{g(\rho_{\mathrm{l}} - \rho_{\mathrm{v}})} \right]^{3/5} v_{\mathrm{l}}^{1/5}, \quad \xi = \frac{11}{16}. \tag{15}$$

2.3. Numerical method to reproduce boiling curves

As described in the previous, although the macrolayer model [1] provided a reasonable assumption on the macrolayer liquid, the method to estimate boiling curve has a problem because it is difficult to determine the relationship between wall superheat and the thickness of macrolayer. Besides this, the boiling curves of saturated liquid except water are difficult to be predicted by their method. However, these problems can be solved well by the present method.

Fig. 2 shows the flow chart for estimating boiling curves. Because the heat flux is the function of wall superheat, from nucleate boiling regime to the CHF, we can obtain the numerical solution of wall superheat by the bisection method. To be specific, initially, for a given heat flux, we obtain the initial macrolayer thickness by Eq. (14). Subsequently, we calculate the heat flux in a certain wall superheat by using the described macrolayer model. Finally, if the difference between the calculated and the given heat flux is less than a decided convergence coefficient, the wall superheat could be considered as the numerical solution of the given heat flux.

The CHF is determined by the following condition as

$$\left| \frac{q_{\mathrm{av2}} - q_{\mathrm{av1}}}{\Delta T_2 - \Delta T_1} \right| < \varepsilon, \tag{16}$$

where ΔT_1 and ΔT_2 are the calculated wall superheat corresponded to q_{av1} and q_{av2}.

In the transition boiling regime, we employ the extrapolated method to determine the boiling curve. Specifically, the initial macrolayer thickness and the wall superheat are gained through the extrapolated line of the obtained boiling curve in nucleate boiling regime. Afterwards, the heat flux can be calculated through the present model.

2.4. Effect of surface roughness

It is known that vapor stems are associated with each active nucleation site [12,22]. However, it is extremely difficult to simulate how vapor stems are formed from active nucleation sites as well as how cavities are activated. In the study of Maruyama et al. [1] and our first part study (Section 2.3), we assumed that the diameters

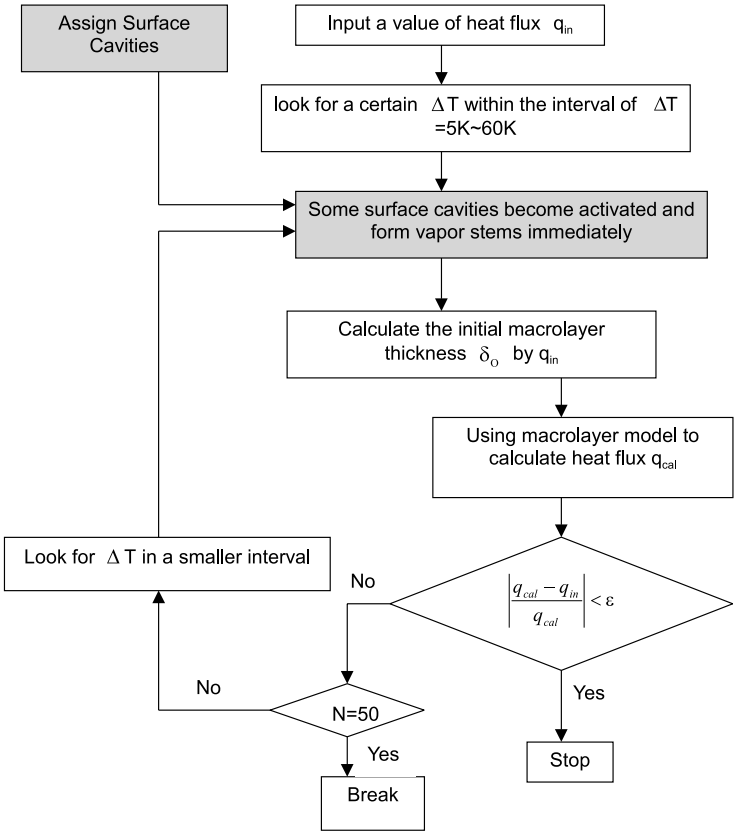

Fig. 2. Flow chart to calculate wall superheat from heat flux.

of vapor stems are not larger than 0.4 mm, hence, according to Eq. 13, the density of active nucleation site is generally constant irrelevant to the wall superheat. Although the initial void fraction is controlled at 1/9, the simulated pattern is inconsistent with the fact that the density of nucleation site density increases with the wall superheat. Thus, we tried to carry out the simulation from the beginning of bubble generation.

So far, there are few studies to characterize the site density quantitatively. Wang and Dhir [26] put forward a correlation about cavity densities and cavity diameters as following:

$$N_s\ (\text{sites/cm}^2) = \begin{cases} 9.0\times10^3 D_c^{*-2.0} & D_c^* \leqslant 5.8\ \mu\text{m}, \\ 10.3 + 2.4\times10^6 D_c^{*-5.2} & 3.5 \leqslant D_c^* < 5.8\ \mu\text{m}, \\ 2213.5 + 1.0\times10^6 D_c^{*-5.4} & D_c^* \leqslant 3.5\ \mu\text{m}. \end{cases} \quad (17)$$

According to the above correlation, the cavity density will be so large that it is impractical to be simulated by the present computer. Hence, referring to the methods described by Shoji [19] and Sadasivan et al. [27], we employed the following method:

1. The number of surface cavities within 100 mm^2 area is set to vary from 150 to 600.
2. By referring to Eq. (17), we set that the cavity diameters are less than 7.0 μm. Among them, 1–5% of the surface cavities is between 5.8 and 7.0 μm, 9–20% is between 3.5 and 5.8 μm and 75–90% is less than 3.5 μm.
3. The site spatial distribution and diameter are assigned randomly by satisfying the conditions in step 2.

The simulated cavities are assigned and distributed in the 21×21 subdivisions. For simplification, we assume that there is atmost one cavity in one mesh and only the biggest one is chosen to be the potential nucleation site. Consequently, a part of assigned cavities is selected to be the potential nucleation sites. The corresponded active wall superheat could be obtained from the following expression:

$$\Delta T_{act} = \frac{2\sigma T_{sat}}{\rho_v H_{fg} R_{ca}}. \quad (18)$$

As shown in Fig. 2, when a certain power is input to the heater, some part of potential nucleate sites becomes activated and forms vapor stems instantaneously. Later,

combining the macrolayer model described before, we could find the wall superheat corresponded to the input heat flux.

3. Application of the model by numerical simulation

3.1. Simulation of transient boiling process

Serizawa [28] put forward a first comprehensive theoretical model to describe transient CHF under power transients. The mechanism of transient CHF is defined as four processes: (a) formation of liquid layer, (b) onset of critical state, (c) stable vapor–liquid configuration destroyed, (d) dry-up of the liquid layer. In the model, although liquid layer thickness was concluded to be a primary influence on the transient burnout behavior, it should be noted that this model is based on a continuous liquid supply to the macrolayer that contradicts the physical evidence presented by Katto and Yokoya [25]. In addition, the surface temperature is assumed to follow the steady-state nucleate boiling and the effect of conduction within the heater is neglected. Furthermore, in determining the liquid layer thickness, it is needed to predict the dry area fraction and other related parameters which are difficult to estimate theoretically. Hence, their argument in the model is confined to water only.

Pasamehmetoglu et al. [29] provided a model for predicting transient CHF in saturated pool boiling. In this model the analysis of heat conduction within the heater is added and is coupled with a macrolayer-thinning model. The prediction indicates a favorable agreement with the experimental data except the fast transient when the exponential period of heat generation rate τ_m is less than 20 ms. However, the prediction was only compared to that of the heater of small diameter wires. In fact, the analytical model is based on the assumption that, for the CHF, the vapor bubble departs only when the macrolayer is dried out completely. This is inconsistent with the experiment by Kirby and Westwater [30]. Zhao et al. [31] recently put forward a model for transient pool boiling heat transfer based on their microlayer model [14]. In their model for predicting CHF [14], the evaporation of the microlayer below the individual bubbles is considered to play an important role in the nucleate boiling heat transfer. For the transient heating, they assume that the population of individual bubbles increases with time and a new group of bubbles with the same size are formed and grow up in each time-step. The transient heat flux is also mainly due to the partial dry out of liquid micolayer underneath individual bubbles. However, their model [31] may be more suitable to the situation of extremely rapid heating, where the formation of vapor mass becomes difficult.

The present model is applied in the transient boiling. Some assumptions are included as follows:

1. The macrolayer establishes immediately when the vapor mass departed from the surface. The motion pictures of Katto and Yokoya [32] showed that the liquid supply was initiated before the formation of vapor mass, however, the delay time of the new vapor bubble is much smaller than the bubble hovering period. Hence, it seems to be reasonable to make this assumption.
2. The initial thickness of the macrolayer is determined by the surface heat flux when the vapor mass takes off. In the transition-boiling regime, the initial thickness of macrolayer is also determined by the extrapolated value of the obtained nucleate boiling curve, which is the same method in determining the transition-boiling heat flux for steady-state.
3. The initial void fraction is not changed with wall temperature. Although the active site population increases with the wall superheat, the product of active site density and diameter of the vapor stem changes little with the wall superheat [21]. Therefore, the assumption may be reasonable. Besides the evaporation of macrolayer at heated surface, one-dimensional transient heat conduction within the heater is also considered. The heat conduction equation is

$$\frac{\partial T}{\partial t} = \alpha_1 \frac{\partial^2 T}{\partial x^2}. \tag{19}$$

Subjecting to the following initial and boundary conditions:

$$t = 0, \quad q_s = q_0, \quad T_w = T_0, \tag{20}$$

$$x = 0, \quad -\lambda \frac{T}{\partial x} = q_s, \tag{21}$$

$$x = H, \quad -\lambda \frac{\partial T}{\partial x} = q_{in}. \tag{22}$$

Employing explicit FDM, we can obtain the instantaneous surface temperature according to the Eqs. (19)–(22).

3.2. Spatial temperature distributions

The three-dimensional transient heat conduction is considered in this part of study. Boiling process is included through boundary conditions. The transient heat conduction is described in Cartesian coordinates as

$$\frac{\partial T}{\partial t} = \alpha_1 \left(\frac{\partial^2 T}{\partial x^2} + \frac{\partial^2 T}{\partial y^2} + \frac{\partial^2 T}{\partial z^2} \right) + \frac{w}{\rho c} \tag{23}$$

Subject to the following boundary and initial conditions:

$$x = 0 \text{ and } x = L, \quad \text{for all } y, z, t \ \frac{\partial T}{\partial x} = 0, \tag{24}$$

$$y = 0 \text{ and } y = L, \quad \text{for all } x, z, t \ \frac{\partial T}{\partial y} = 0, \tag{25}$$

$$z = H, \quad -\lambda_H \frac{\partial T}{\partial Z} = q_b, \tag{26}$$

$$z = 0, \quad q_s(i,j) = -\lambda_H \left(\frac{\partial T}{\partial z} \right). \tag{27}$$

The first four boundary conditions for the y and x directions are referred to as a representative rectangular portion of the total heater, where the periphery acts as a symmetry line. The boundary condition of the bottom is shown in Eq. (26). At this condition, the heat generation term $w/\rho c$ in Eq. (23) is set to zero. Eq. (27) shows the boundary condition at the top of heater. As the top of the heater is the boiling surface, the boiling effects are included through calculating the local surface heat flux of boiling. The local surface heat flux $q_s(i,j)$ can be calculated by Eq. (10). In addition, the initial condition is specified as

$$T_s(i,j) = T_0. \tag{28}$$

The initial temperature profile inside the heater is calculated by one-dimensional steady-state heat conduction, i.e.,

$$T(i,j,k) = T_s(i,j) + \frac{k\Delta z}{\lambda_H} q_{in}. \tag{29}$$

The fully implicit scheme is employed to the three-dimensional heat conduction problem. Although the fully implicit scheme for the heat conduction is stable at any time, there is a limitation when it is combined with the calculation of pool boiling heat transfer. The calculation is stable when the following condition is satisfied:

$$t\Delta T_t \leqslant (t + \Delta t)\Delta T_{t+\Delta t} \tag{30}$$

4. Results and discussion

4.1. Boiling curves and the dependence of parameters

The diameter of simulated area is 10 mm. Fig. 3 shows the estimated boiling curve of water. We can see that the prediction in the high heat flux regime is in a good agreement with the experiments, however, it predicted higher in the low heat flux regime. This implies that this model is more suitable for the high heat flux regime. The CHF predicted by the present simulation is 1.63 MW/m^2 at $\delta_0 = 38$ μm, which is almost the same as that estimated by Katto and Yokoya [25].

The boiling curve of FC-72 is also calculated. The fluid is saturated at a temperature of 329 K. The averaged bubble departure period of FC-72 is 30 ms which is calculated from Eq. (14). Until now, we have some information about the diameter of vapor stem for water (Eq. (13)), but few is for FC-72. Thus, we assume that Eq. (13) is also fulfilled for FC-72. This is expected to be reasonable because the growth of void fraction is more important than void fraction itself (from Figs. 5 and 7, we can know that $q_\alpha > q_\delta$. Meanwhile Eq. (10) shows that $q_\delta \propto (1-\alpha)(-\mathrm{d}\delta/\mathrm{d}t)$ and $q_\alpha \propto \delta(\mathrm{d}\alpha/\mathrm{d}t)$). The

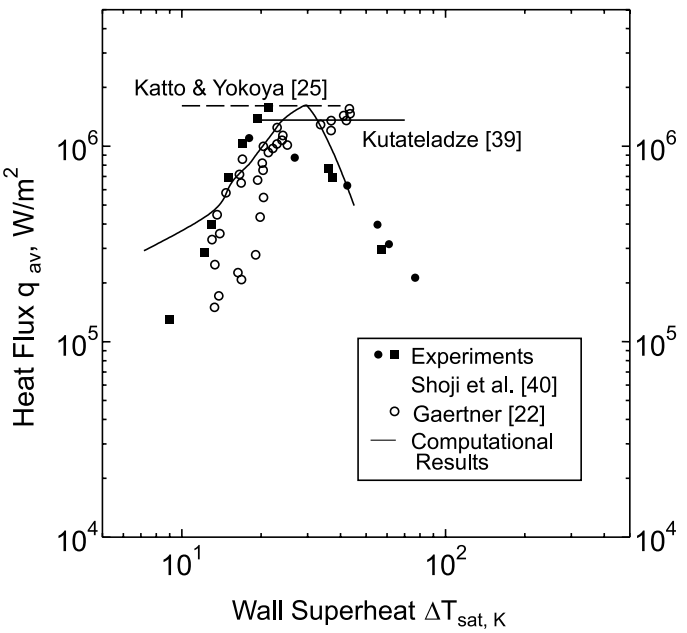

Fig. 3. Simulated boiling curve of water.

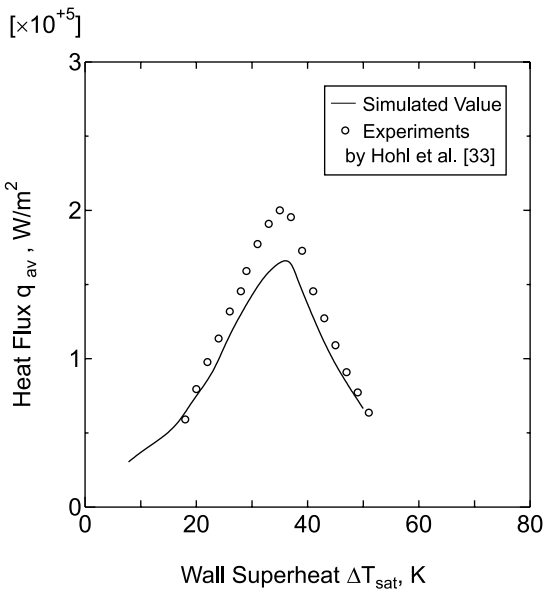

Fig. 4. Simulated boiling curve of fluorinert FC-72.

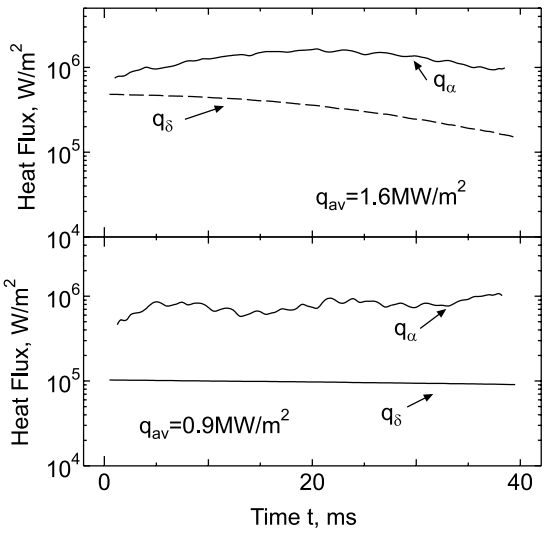

Fig. 5. Variations of q_α and q_δ for different averaged heat flux.

results are plotted in Fig. 4. We can see that except the lower CHF, they are almost consistent with the experimental values carried out by Hohl et al. [33]. The predicted CHF by the present model is $q = 1.7 \times 10^5$ W/m^2 at $\Delta T = 36$ K. The CHF calculated by Eq. (1) is 1.4×10^5 W/m^2. Thus, we believe that the predicted value is reasonable.

Table 1 provides the relative evaporation contributions to the total heat flux. Column 3 shows the ratio of $\bar{q}_\alpha$ to the total averaged heat flux q_{av} and column 4 is the ratio of $\bar{q}_\delta$ to q_{av}. It can be seen in the table that the value of $\bar{q}_\alpha/q_{\mathrm{av}}$ is larger than that of $\bar{q}_\delta/q_{\mathrm{av}}$. Additionally, with the increase of total averaged heat flux, $\bar{q}_\alpha/q_{\mathrm{av}}$ becomes smaller but $\bar{q}_\delta/q_{\mathrm{av}}$ becomes larger (from 0.034 to 0.212). This suggests that the evaporation of vapor stem–macrolayer interface is the main part for the total evaporation. On the other hand, with the increasing of heat flux, or with the thinning macrolayer thickness, the evaporation of vapor bubble–liquid layer interface plays a more important role than that at lower heat flux.

Fig. 5 gives the variation of q_δ and q_α with time when the average heat flux is 1.6 and 0.9 MW/m^2, respectively. As displayed there, for the same average heat flux, q_α is always larger than q_δ at any time.

According to the method described in Section 2.4, we obtained the predicted boiling curves for different surface conditions. As displayed in Fig. 6, with the number of cavities increasing, the boiling curves move the lower superheat region, whereas the CHF value does not change significantly. When the number of surface cavities is 600, for relatively rougher surface, the boiling curve shifts to the left of the curve for smoother surface. This indicates the same tendency of Bereson's experimental results [34].

Fig. 7 shows the variations of heat flux q_α, q_δ and q when the average heat flux is 1.6 MW/m^2. We can see that the heat flux component q_δ (related to the decay of macrolayer thickness) when $N_s = 600$ is smaller than that without considering surface cavities, whereas the heat flux component q_α (related to the growth of vapor stems) when $N_s = 600$ is larger (from Eq. (10)). Hence, the heat flux q when $N_s = 600$ does not change considerably compared to the heat flux without considering surface

Table 1
Comparison of relative heat flux $\bar{q}_\alpha/q_{\mathrm{av}}$ and $\bar{q}_\delta/q_{\mathrm{av}}$ for different averaged heat flux

Averaged heat flux q_{av} (MW/m^2)	Wall super heat ΔT_{sat} (K)	Relative heat flux $\bar{q}_\alpha/q_{\mathrm{av}}$	Relative heat flux $\bar{q}_\delta/q_{\mathrm{av}}$
0.387	14.3	0.966	0.034
0.713	18.9	0.922	0.078
0.996	21.6	0.89	0.11
1.165	23.5	0.856	0.144
1.44	26.4	0.82	0.18
1.58	29.9	0.788	0.212

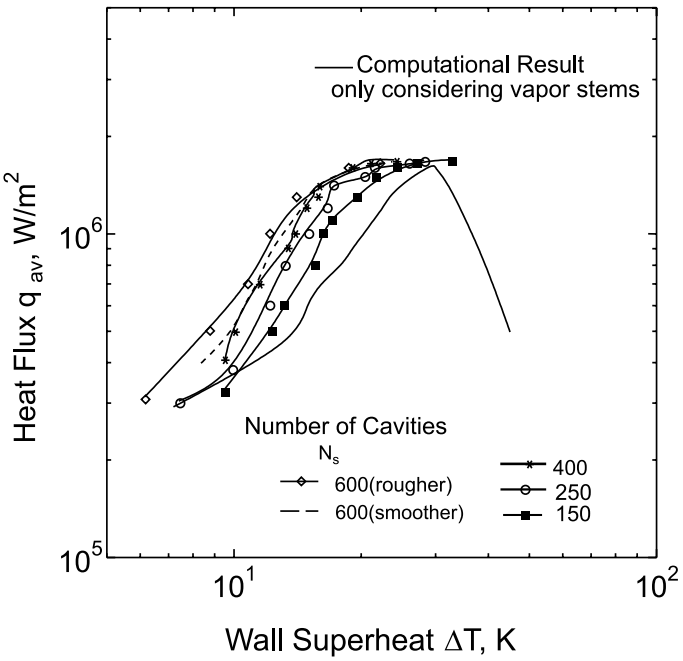

Fig. 6. Predicted boiling curves for different surface conditions.

cavities. Thus, we can conclude that the variation of surface roughness affects the heat flux component rather than the total heat flux. That is, the heat flux related to the evaporation of macrolayer thickness becomes smaller and the heat flux related to the growth of vapor stems becomes larger when surface roughness increases.

4.2. Results of transient heating

The input heat flux was set to increase linearly and exponentially. The incipient boiling superheats of water and FC-72 were set at 10 and 15 K, respectively [35,36]. The simulated area was 10 mm in diameter and the heater was copper with 10 mm in thickness. The bubble departure periods of water and FC-72 are calculated by Eq. (15). As the bubble departure periods do not change extensively with heat flux according to Huang [35], we employed the averaged values as 40 and 30 ms for water and FC-72, respectively. The averaged transient heat flux increases with time and reaches the peak value automatically.

The wall temperature variation when the heating rate is zero is investigated. The result is plotted in Fig. 8. In nucleate boiling regime ($T_w = 122°C$), the variation is extremely small. With the wall superheat increasing, the fluctuation becomes larger, especially in transition boiling regime. This is because the macrolayer is considerably thin and is consumed completely within a short period.

The transient boiling curves of water and FC-72 are plotted in Figs. 9 and 10. From these two figures, we can see that the boiling curves change with the heating rates. For lower transients, boiling curves almost remain the same as the steady-state curve. Beyond the steady-state CHF, the nucleate boiling curves extend until the transient CHF is reached. For higher transient heating rate, the boiling curves deviate from the steady-state curve and the CHF becomes much higher. The experimental data by Hohl et al. [36] are also plotted in Fig. 10. It is found that the simulated results have the same tendency as the experimental data. In their experiment [36], the diameter of heater was 34 mm, this may be the reason that the CHF values are higher than the simulated results.

The transient boiling curves of water with increasing heat input exponentially are plotted in Fig. 11(a). Referred to the experiments by Sakurai and Shiotsu [37], the exponential periods are varied from 5 s to 50 ms. It shows the same characteristics as that shown in Fig 10. The variation of transient CHF with time is plotted in Fig. 11(b). It can be seen that transient CHF generally increases with the heating rate. This tendency is the same as that by Sakurai and Shiotsu's experiment on a thin wire [37]. However, it is remarked that transient CHF appears to fluctuate when the exponential period t_0 is less than 70 ms. This implies that the transient boiling becomes irregular when the exponential period is less than 70 ms. In the simulation, the transient heat flux is

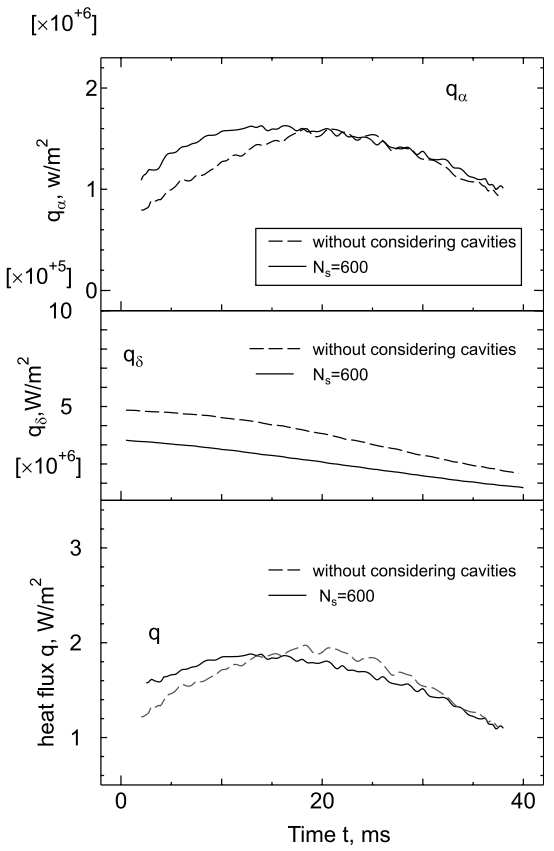

Fig. 7. Variations of q_α, q_δ and q with time when average heat flux $q_{av} = 1.6$ MW/m^2 (without considering cavities and $N_s = 600$).

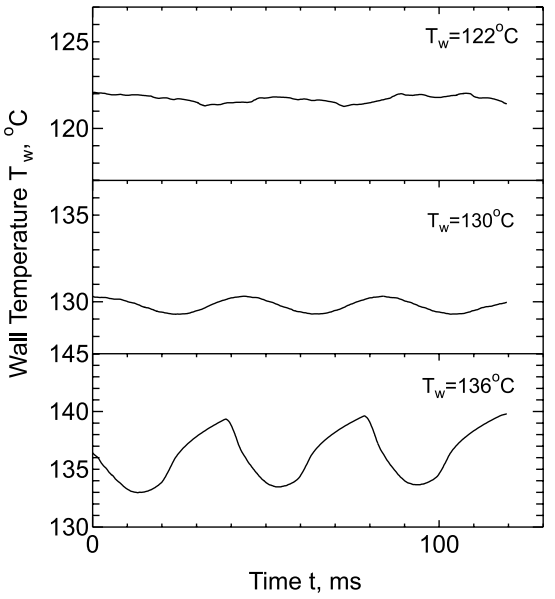

Fig. 8. Wall temperature variations in different boiling regimes.

related to the conduction within the heater, the heat removed from the macrolayer and from liquid–vapor–solid triple point. The fluctuation may be due to the imbalance of heat transfer among them. In fact, Sukurai and Shiotsu [37] have observed that, at atmospheric pressure, the boiling becomes to fluctuate when the exponential period is less than 50 ms. With the pressure becoming higher, the fluctuation tends to be less and the exponential period where the fluctuation appears becomes shorter. At present, we just confined the situation at atmospheric pressure, further consideration is needed for studying higher pressures.

We can do further investigation by plotting the variations of α, δ, q_α and q_δ for steady-state and transient heating. Fig. 12(a) shows the changes of macrolayer thickness, and Fig. 12(b) shows the changes of void fraction of point 1 (steady-state) and point 2 (transient heating) in Fig. 9. It is revealed that the macrolayer thickness of point 2 is thicker than that of point 1, whereas the instantaneous void fraction α of point 2 is a little less than that in point 1.

Fig. 13 provides the variations of q_α and q_δ for steady-state and transient heating. It shows that q_α of transient heating at 80 K/s heating rate is larger than or equal to that of steady-state, whereas q_δ at 80 K/s changes little as compared to the steady-state curve. Since $d\alpha/dt$ at 80 K/s heating rate is less than $d\alpha/dt$ at steady-state (Fig. 12), from Eq. (10), we can conclude that because of the increase of macrolayer thickness, the transient CHF increases. This conclusion is in an agreement with that drawn by Serizawa [28], however, Serizawa' s model [28] is based on a continuous liquid supply to the macrolayer, which is different from the present model (cf. Section 3.1).

4.3. Spatial temperature distribution

Fig. 14(a) shows the surface pattern at 0.5 and 30 ms when the average heat flux is 1.57 MW/m^2. The thickness of the heater is 1 mm. Fig. 14(b) gives the temperature variations of five points signed in 14(a) within two bubble departure periods. We can see that, when vapor and liquid are filled with the grids at the same time, the temperatures in these points are generally lower; when only vapor or liquid occupies the grids, the temperatures are relatively higher.

Fig. 15 provides the local instantaneous temperatures on the whole surface at 0.5 and 30 ms. Compared to Fig 14(a), it is revealed that the surface temperatures remained almost the same at the initial stage of the hovering period. The low temperature points are the place, where liquid and vapor exist at the same grid. With the time increasing, the areas that liquid and vapor

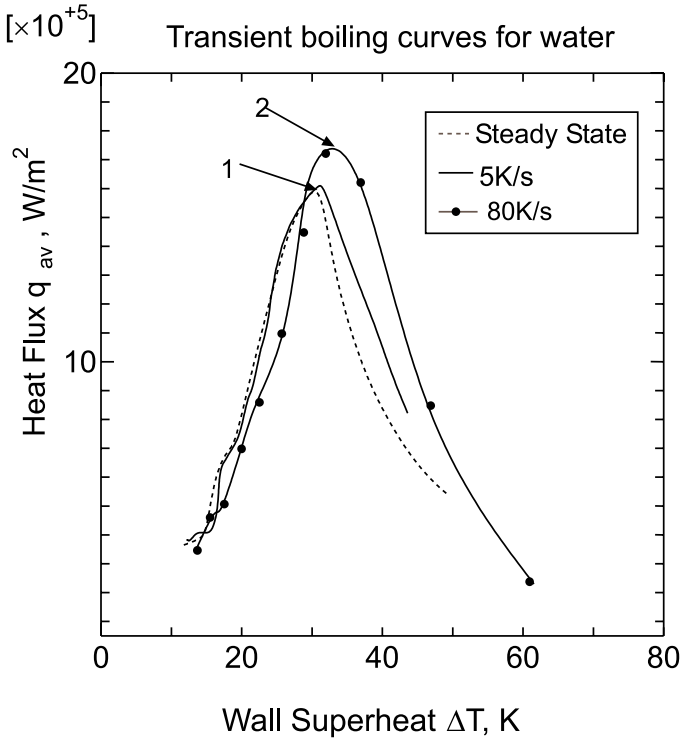

Fig. 9. Predicted transient boiling curves of water.

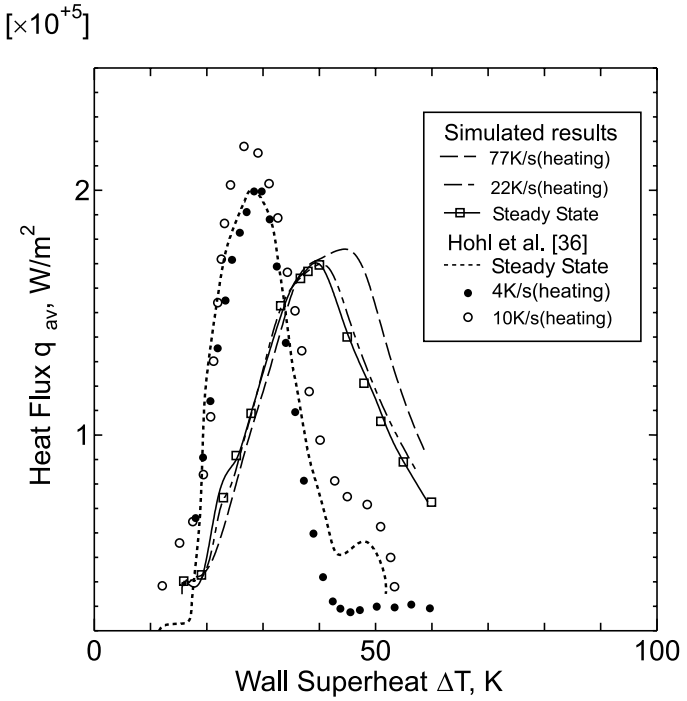

Fig. 10. Simulated transient boiling curves of FC-72 for different heating rates.

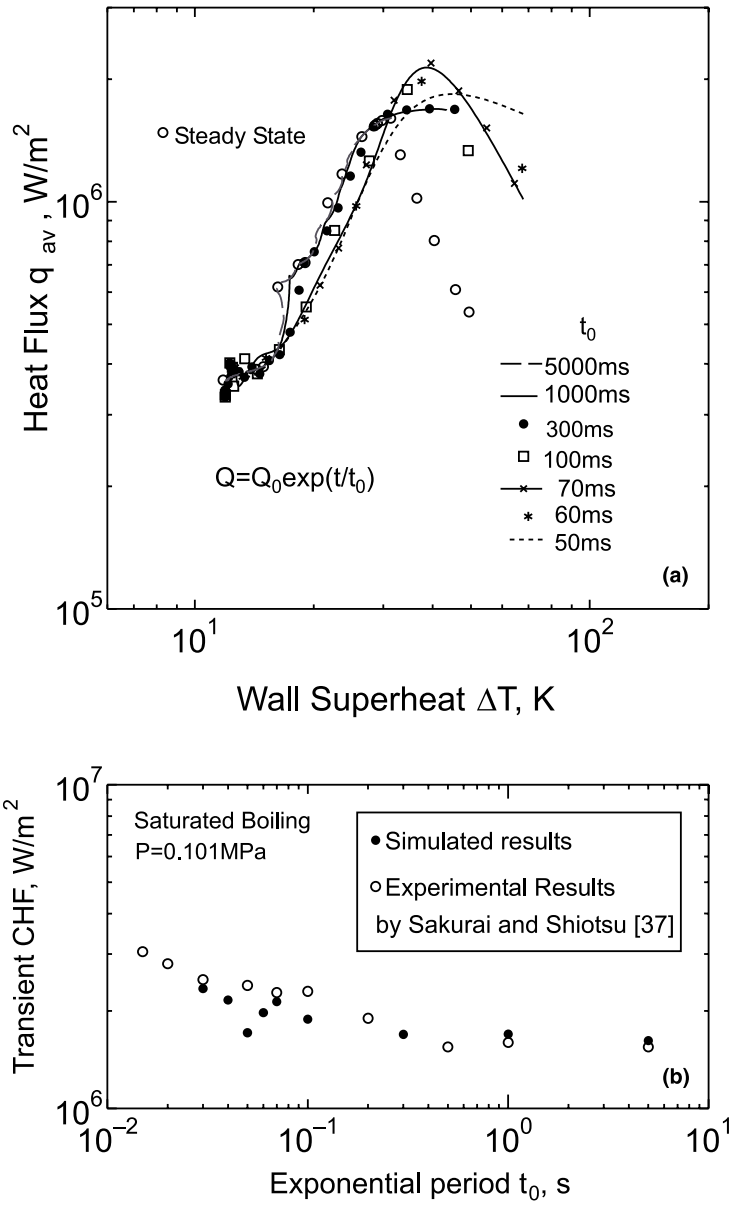

Fig. 11. Predicted results by exponential heating increase: (a) transient boiling curves; (b) relationship between transient CHF and exponential period.

intersect become more, whereas the areas that only liquid or vapor is filled with are less. Hence, the places where the surface temperatures changed considerably become so much more that the temperature in the whole surface varied greatly.

In summary, the lowest temperature point at a certain time is always at the vapor–liquid interface. This result is consistent with the deduction by Pasamehmetoglu et al. [38]. The temperature in the places where the vapor–liquid interface does not pass through are usually higher.

5. Summary and conclusion

In this study, through several numerical methods, the numerical macrolayer model [1] was developed significantly. The main conclusions can be drawn as follows:

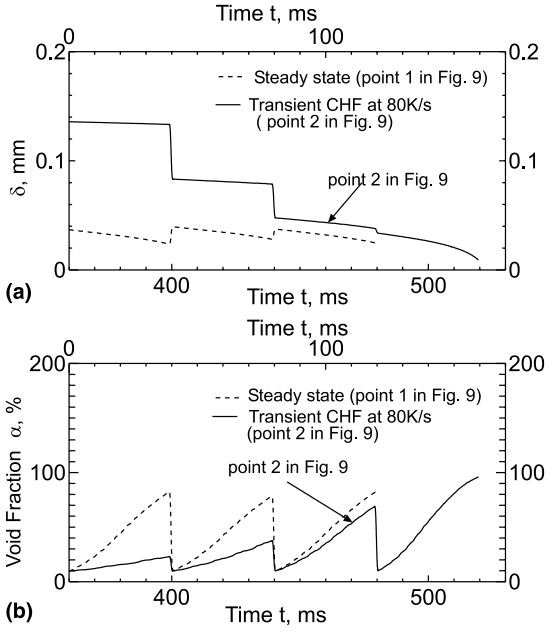

Fig. 12. Comparison of characteristic parameters for transient boiling and steady-state: (a) changes of macrolayer thickness; (b) changes of void fraction.

1. The present model can explain steady-state boiling quantitatively.

   (a) In this study, by using bisection method, the boiling curves of water and FC-72 are obtained. The simulated CHF is favorably consistent with the value calculated by Katto and Yokoyo's equation [25]. It is slightly higher than the value predicted by Kutateladze [39]. The simulated results for higher heat fluxes are in a good agreement with the available experimental data [22,40]. For lower heat flux, the predicted results are higher than the experimental results.

   (b) Generally, the evaporation due to the growth of vapor stem is the main contribution to the total heat flux. With the increasing of heat flux, the evaporation due to the decay of macrolayer plays a more important role in the total heat flux (cf. Table 1, Figs. 5, 7 and 13). This is in agreement with the conclusion of the model by Pasamehmetoglu et al. [38] and is consistent with the observations by Nagai and Nishio [13].

   (c) The boiling curve shifts to the left with the increase of surface roughness, whereas the CHF value only slightly changes with surface roughness. This is in an agreement with the experimental

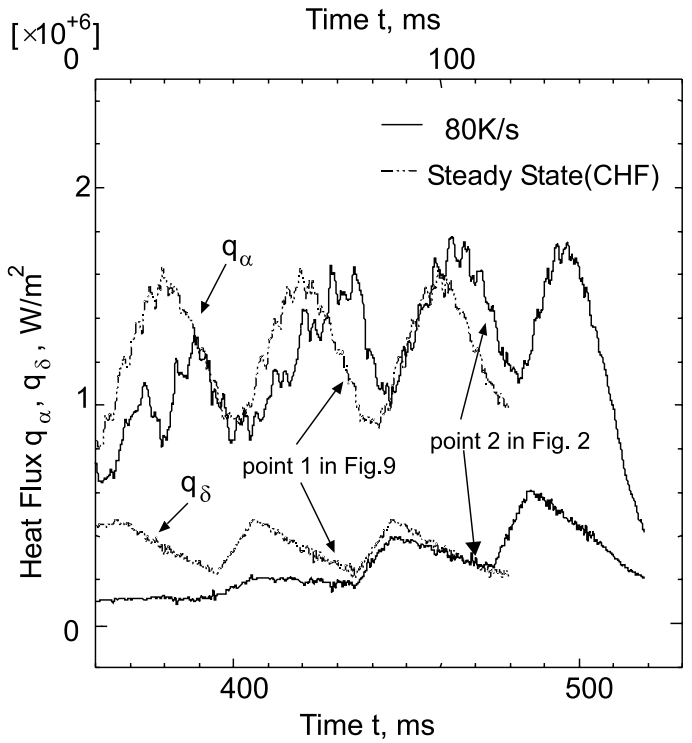

Fig. 13. Comparison of q_α and q_δ for transient boiling and steady-state.

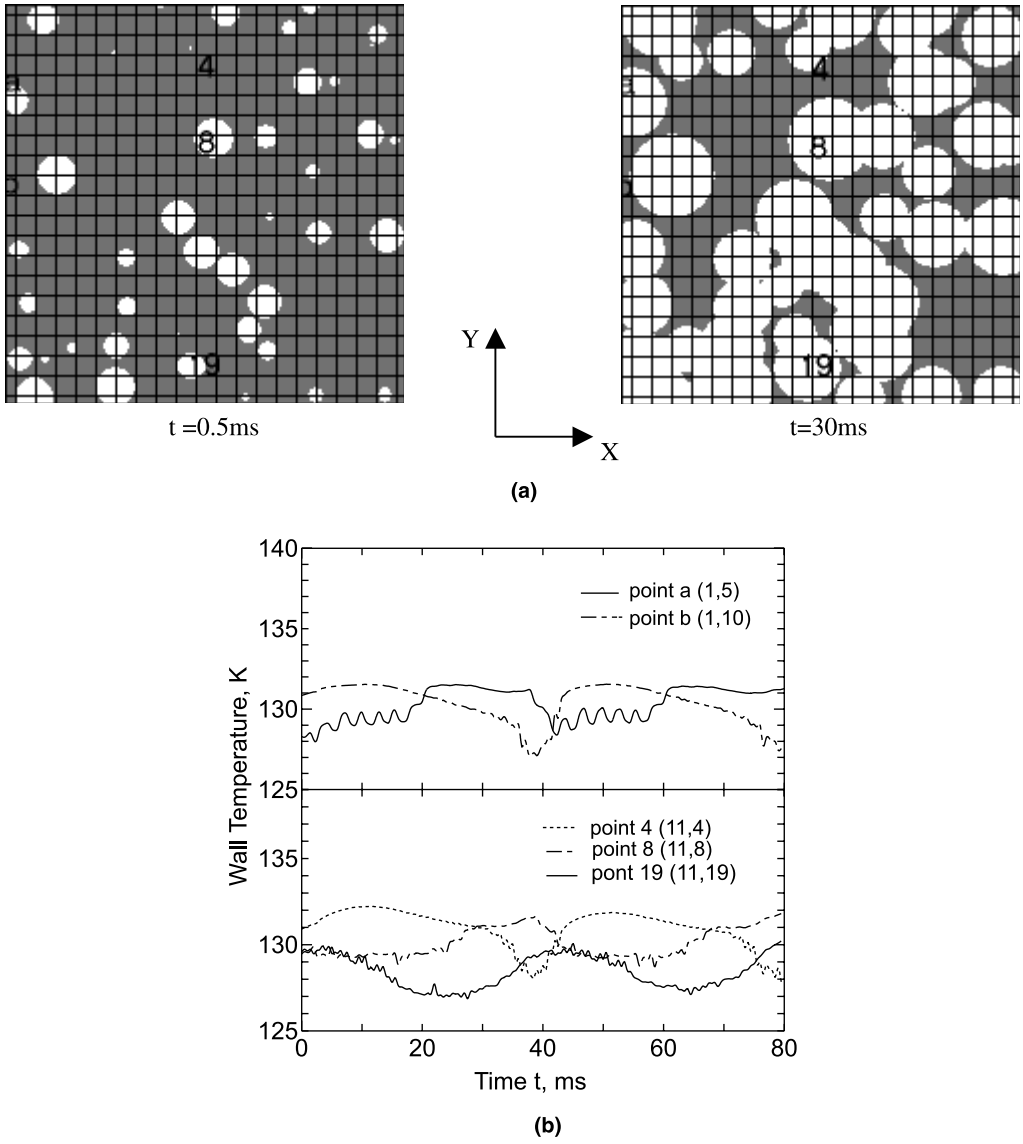

Fig. 14. (a) Instantaneous surface dry pattern; (b) temporal variations of instantaneous wall temperatures for different positions ($q = 1.57$ MW/m^2, $H = 1$ mm).

result of Berenson [34] qualitatively. It is found that the little variation on the CHF value when the surface roughness increases is because the evaporation due to decay of macrolayer declines and the evaporation due to growth of vapor stems becomes increased.

(d) Through the investigation of spatial temperature distribution, it is shown that the low temperature point is generally in the place where vapor and liquid phase occupy at the same time, whereas in the place where only vapor or liquid is filled, the temperature is relatively higher. This also proves that the evaporation at the interface of vapor stem–liquid is the main part of the total heat flux.

2. The present model can explain transient boiling qualitatively.

   (a) The macrolayer model is extended to transient boiling. Combining the present developed model and one-dimensional transient heat conduction within the heater, transient boiling curves of water and FC-72 by increasing input heat linearly are obtained. The results give the same tendency as the experimental results of Hohl et al. [36].

   (b) Transient boiling curves are obtained by increasing input heat exponentially. They show the

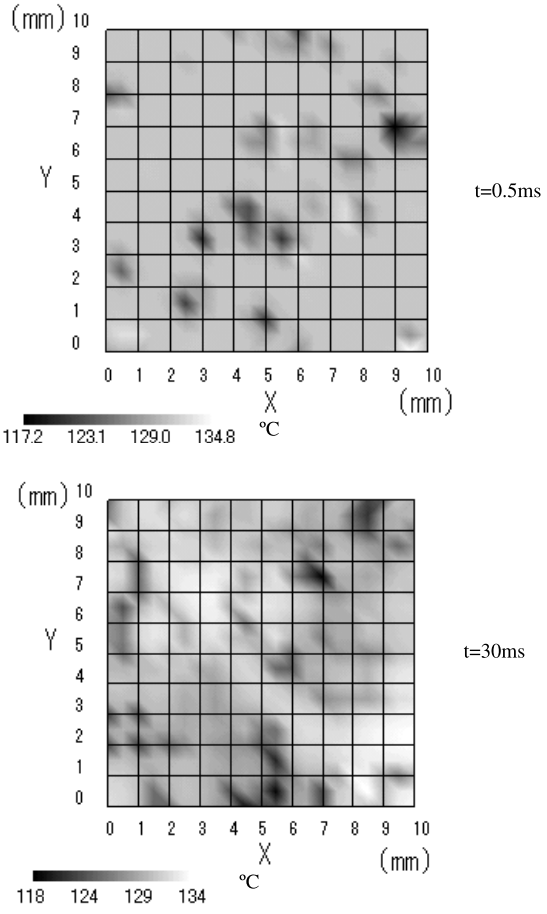

Fig. 15. Local instantaneous temperatures on the heated surface ($q = 1.57$ MW/m^2, $H = 1$ mm).

same tendency as the experimental results of Sukurai and Shiotsu [37].

(c) It is displayed that the macrolayer plays an important role in increasing the transient CHF.

References

[1] S. Maruyama, M. Shoji, S. Shimizu, A numerical simulation of transition boiling heat transfer, in: Proceedings of the Second JSME-KSME Thermal Engineering Conference, 1992, pp. 3-345-3-348.

[2] J.J. Xu, Z.Q. Lu, Boiling Heat Transfer and Gas Liquid Two Phase Flow, Nuclear Energy, Beijing, 1993, pp. 420–422.

[3] V.P. Carey, Pool boiling, in: Liquid-Vapor Phase-Change Phenomena: An Introduction to the Thermophysics of Vaporization and Condensation Process in Heat Transfer Equipment, Hemisphere, Washington, DC, 1992 (Chapter 7).

[4] W.M. Rohsenow, A method correlating heat transfer data for surface boiling liquids, Trans. ASME 84 (1962) 969–978.

[5] N. Zuber, Nucleate boiling. The region of isolated bubbles and the similarity with natural convection, Int. J. Heat Mass Transfer 6 (1963) 53–78.

[6] N. Zuber, Hydrodynamic aspects of boiling heat transfer, AEC Report No. AECU-4439, 1959.

[7] N. Zuber, On the stability of boiling heat transfer, Trans. ASME 80 (1958) 711–720.

[8] Y. Haramura, Y. Katto, A new hydrodynamic model of critical heat flux applicable widely to both pool and forced convection boiling on submerged bodies in saturated liquids, Int. J. Heat Mass Transfer 26 (2) (1983) 389–399.

[9] C. Pan, J.Y. Hwang, T.L. Lin, The mechanism of heat transfer in transition boiling, Int. J. Heat Mass Transfer 32 (1989) 1337–1349.

[10] P. Sadasivan, C. Unal, R.A. Nelson, Perspective: issues in CHF modeling – the need for new experiments, Trans. ASME J. Heat Transfer 117 (1995) 558–567.

[11] A.M. Bhat, R. Prakash, J.S. Saini, On the mechanism of macrolayer formation in nucleate pool boiling at high heat flux, Int. J. Heat Mass Transfer 26 (5) (1983) 735–740.

[12] V.K. Dhir, P. Liaw, Framework for unified model for nucleate and transition pool boiling, Trans. ASME J. Heat Transfer 111 (3) (1989) 739–746.

[13] N. Nagai, S. Nishio, Liquid–solid contact phenomena in boiling heat transfer (proposal of concept of contact-line length density), Trans. JSME B 63 (106) (1997) 220–227.

[14] Y.H. Zhao, T. Masuoka, T. Tsuruta, Prediction of critical heat flux based on the microlayer model, Trans. JSME B 62 (598) (1996) 246–251.

[15] K.O. Pasamehmetoglu, R.A. Nelson, A finite-control volume computer program for heater analysis of nucleation dynamics (HANDY), Los Alamos National Laboratory Report LA-UR-91-977, 1991.

[16] K.O. Pasamehmetoglu, Numerical modeling of a nucleate boiling surface, Num. Heat Transfer: Int. J. Comput. Methodol. Part A: Appl. 25 (6) (1994) 703–719.

[17] Q. Bai, Y. Fijita, Numerical simulation of the growth for a single bubble in nucleate boiling, Thermal Sci. Eng. 7 (4) (1999) 45–52.

[18] G. Son. V.K. Dhir, Numerical simulation of a single bubble during partial nucleate boiling on a horizontal surface, in: Proceedings of 11th IHTC, vol. 2, Kyongju, Korea, 1998, pp. 533–538.

[19] M. Shoji, Boiling simulator: a simple theoretical model of boiling, in: Third International Conference on Multiphase Flow, 0.2-14, Lyon, France, 1998.

[20] M. Shoji, K. Tajima, Mathematical simulation model of boiling: modes and chaos, Convective Flow and Pool Boiling Conference, Session X: Pool Boiling, Kloster Irsee, 1997.

[21] Y. Hashimoto, H. Ohashi, Digital boiling using cellular automata, in: Proceedings of the High Performance Computing on Multiphase Flows, Tokyo, Japan, 1997.

[22] R.F. Gaertner, Photographic study of nucleate pool boiling on a horizontal surface, ASME J. Heat Transfer 87 (1965) 17–29.

[23] M. Shoji, H. Kuroki, Model of macrolayer formation in pool boiling, in: Proceedings of the 10th International Heat Transfer Conference, 1994, pp. 147–152.

[24] A.K. Rajvanshi, J.S. Saini, R. Prakashi, Investigation of macrolayer thickness in nucleate pool boiling at high heat flux, Int. J. Heat mass Transfer 35 (2) (1992) 343–350.
[25] Y. Katto, S. Yokoya, Behavior of a vapor mass in saturated nucleate and transition pool boiling, Trans. JSME 41 (1975) 294–305.
[26] C.H. Wang, V.K. Dhir, Effect of surface wettability on active nucleation site density during pool boiling of water on a vertical surface, Trans. ASME J. Heat Transfer 115 (1993) 659–669.
[27] P. Sadasivan, C. Unal, R. Nelson, Nonlinear aspects of high heat flux nucleate boiling heat transfer, Trans. ASME J. Heat Transfer 117 (1995) 981–989.
[28] A. Serizawa, Theoretical prediction of maximum heat flux in power transients, Int. J. Heat Mass Transfer 26 (6) (1983) 921–932.
[29] K.O Pasamehmetoglu, R.A. Nelson, F.S. Gunnerson, Critical heat flux modeling in pool boiling for steady-state and power transients, J. Heat Transfer Trans. ASME 112 (1990) 1048–1057.
[30] D.B. Kirby, J.W. Westwater, Bubble and vapor behavior on a heated horizontal plate during pool boiling near burnout, Chem. Eng. Prog. Symp. Ser. 61 (57) (1965).
[31] Y.H. Zhao, T. Masuoka, T. Tsuruta, Theoretical studies on transient pool boiling based on microlayer model (mechanism of transition from non-boiling regime to film boiling), Trans. JSME B 63 (607) (1997) 218–223.
[32] Y. Katto, S. Yokoya, M. Yasunaka, Mechanism of boiling crisis and transition boiling in pool boiling, in: Proceedings of the Fourth International Heat Transfer Conference, vol. 5, Paris, 1970, pp. B3.2.
[33] R. Hohl, H. Auracher, J. Blum, Identification of liquid–vapor fluctuations between nucleate and film boiling in natural convection, in: Convective Flow and Pool Boiling Conference, Section II : Pool Boiling, Kloster Irsee, 1997.
[34] P.J. Berenson, Transition boiling heat transfer from a horizontal surface, M.I.T Heat Transfer Lab. Tech. Rep. 17, 1960.
[35] Z.L. Huang, A study of steady transition boiling of water, Ph.D. thesis, Faculty of Engineering, The University of Tokyo, 1993.
[36] R. Hohl, H. Auracher, J. Blum, W. Marquardt, Pool boiling heat transfer experiments with controlled wall temperature transients, in: Proceedings of the Second European Thermal Science and 14th UIT National Heat Transfer Conference, vol. 3, 1996, pp. 1647–1652.
[37] A. Sakurai, M. Shiotsu, Transient pool boiling heat transfer part 2: boiling heat transfer and burnout, ASME J. Heat Transfer 99 (1977) 554–560.
[38] K.O. Pasamehmetoglu, P.R. Chappidi, C. Unal, R.A. Nelson, Saturated pool nucleate boiling mechanism at high heat fluxes, Int. J. Heat Mass Transfer 36 (15) (1993) 3859–3868.
[39] S.S. Kutateladze, On the transition to film boiling under natural convection, Kotloturbostroenie 3 (1948) 10.
[40] M, Shoji, Study of steady transition boiling of water: experimental verification of macrolayer evaporation model, in: Proc. Eng. Found. Conf. Pool External Flow Boiling, ASME, New York, 1992, pp. 237–242.